Article

Energy Consumption Analysis for Continuous Phase Modulation in Smart-Grid Internet of Things of beyond 5G

Hongjian Gao [1], Yang Lu [1], Shaoshi Yang [2,3,*], Jingsheng Tan [2,3], Longlong Nie [2,3] and Xinyi Qu [2,3]

[1] State Grid Smart Grid Research Institute Co., Ltd., Beijing 102209, China; jangseohee1987@aliyun.com (H.G.)
[2] School of Information and Communication Engineering, Beijing University of Posts and Telecommunications, Beijing 100876, China
[3] Key Laboratory of Universal Wireless Communications, Ministry of Education, Beijing 100876, China
[*] Correspondence: shaoshi.yang@bupt.edu.cn

Abstract: Wireless sensor network (WSN) underpinning the smart-grid Internet of Things (SG-IoT) has been a popular research topic in recent years due to its great potential for enabling a wide range of important applications. However, the energy consumption (EC) characteristic of sensor nodes is a key factor that affects the operational performance (e.g., lifetime of sensors) and the total cost of ownership of WSNs. In this paper, to find the modulation techniques suitable for WSNs, we investigate the EC characteristic of continuous phase modulation (CPM), which is an attractive modulation scheme candidate for WSNs because of its constant envelope property. We first develop an EC model for the sensor nodes of WSNs by considering the circuits and a typical communication protocol that relies on automatic repeat request (ARQ)-based retransmissions to ensure successful data delivery. Then, we use this model to analyze the EC characteristic of CPM under various configurations of modulation parameters. Furthermore, we compare the EC characteristic of CPM with that of other representative modulation schemes, such as offset quadrature phase-shift keying (OQPSK) and quadrature amplitude modulation (QAM), which are commonly used in communication protocols of WSNs. Our analysis and simulation results provide insights into the EC characteristics of multiple modulation schemes in the context of WSNs; thus, they are beneficial for designing energy-efficient SG-IoT in the beyond-5G (B5G) and the 6G era.

Keywords: continuous phase modulation (CPM); wireless sensor network (WSN); energy efficient; modulation optimization; smart grid; Internet of Things (IoT); B5G; 6G

1. Introduction

Smart grid is the energy infrastructure for smart cities, telecommunications, networks, and the computing industry. It upgrades traditional power grid systems with state-of-the-art information and communication technologies, such as wireless sensor network (WSN) techniques and the Internet of Things particularly designed for the smart grid industry (SG-IoT). In fact, SG-IoT heavily relies on WSN, which is characterized by a variety of distinct performance metrics, such as transmission rate, signal coverage, energy consumption (EC), and network lifetime [1]. Among all these metrics, it is of particular importance to place emphasis on the EC (defined as the number of joules consumed per successfully transmitted bit) of wireless sensors, because the energy supply requirements of sensors are stringent in WSNs (i.e., very limited energy supply) and all the other performance metrics can be affected by the EC characteristic of sensors. To elaborate a little further, in many application scenarios of the smart grid industry, it is often inconvenient or unsafe for humans to work in the deployment site and the lifetime of sensors is often expected to be over several years. Therefore, low EC is of vital importance for these scenarios.

By contrast, in wireless communication systems that operate with the support of power grid infrastructure, it is more appropriate to invoke energy efficiency (EE), which

is typically defined as the number of bits successfully transmitted per joule. This concept is at the heart of green communications, a vision globally recognized for reducing the Carbon footprint produced by the networking sector, especially in the era of 5G, 5G-Advanced, and 6G [2]. Obviously, EE is the reciprocal of EC. Extensive studies have been devoted to optimizing the EE of wireless networks in the past decade. For instance, in [3], based on the fractional programming framework, the joint power and subcarrier allocation problem was solved for maximizing the EE of a multi-user, multi-relay, single-cell orthogonal frequency-division multiple access (OFDMA) cellular network composed of single-antenna nodes. Afterwards, system models that are more complicated were considered: the joint transmit and receive beamforming-based multi-user, multi-relay, multi-input multi-output (MIMO)-OFDMA cellular networks [4,5]; the multi-cell single-antenna OFDMA networks [6]; the partial/full interference alignment-based multi-user, multi-relay, multi-cell MIMO-OFDMA networks [7]; the massive MIMO-aided, multi-pair, one-way decode-and-forward relay system [8]; and the fully connected *K*-user interference channel with each user having either a single antenna or multiple antennas [9]. Additionally, the EE of wireless networks that are delay-sensitive was also studied by maintaining statistical quality-of-service QoS guarantees in OFDMA networks [10] and by considering the uplink ultra-reliable low-latency communication (URLLC) traffic in the MIMO-aided grant-free access [11] of 5G and its beyond. In [12], secrecy-energy efficient hybrid beamforming schemes were designed for a satellite-terrestrial integrated network in order to maximize the achievable secrecy-EE while satisfying the signal-to-interference-plus-noise ratio (SINR) constraints of both the earth stations and the cellular users; further, in [13], the secrecy-energy efficient beamforming in multibeam satellite systems was investigated with the metric of signal-to-leakage-plus-noise ratio (SLNR).

Since wireless sensors are typically powered by batteries, it is more appropriate to use EC in the context of wireless sensors. EC is closely related to the selected modulation scheme. Firstly, this selection may influence the type of electronic components utilized, such as a power amplifier (PA) or analog-to-digital converter (ADC), because different modulation schemes may require different circuit designs and implementations. Secondly, the specific choice of modulation schemes also affects the number of bits transmitted in a single symbol duration that consumes a certain amount of energy. Thirdly, different modulation schemes may incur different packet error rates (PERs), which influence the number of retransmissions that also consume energy and are necessary for successful packet delivery between any pair of wireless sensors. Therefore, it is important to investigate the impact of different modulation schemes on the EC and identify the most appropriate scheme for WSNs of SG-IoT.

Prior research mainly focused on studying the EC of modulation schemes that are sensitive to the nonlinearity of PAs. More specifically, in [14], the EC minimization problems corresponding to *M*-ary quadrature amplitude modulation (MQAM) and multiple frequency-shift keying (MFSK) were studied. In [15,16], the authors studied the relationship between the total EC per successfully transmitted information bit and the transmission distance while assuming different modulation methods, such as binary phase-shift keying (BPSK), quadrature phase-shift keying (QPSK), and 16QAM. They also studied the average signal-to-noise ratio (SNR) values required to achieve the optimal EC. In [17], the transmission power of MQAM was optimized by using a particular model to achieve the minimum EC. In [18], the EC per successfully transmitted bit for modulation techniques including binary frequency-shift keying (BFSK), BPSK, QPSK, 16QAM, and 64QAM was studied under various channel conditions. However, these modulation techniques require the use of linear PAs, which results in lower energy utilization efficiency. In contrast, constant envelope modulation techniques are insensitive to the nonlinearity of PAs; thus, they constitute a promising solution to improving the energy utilization efficiency. However, there is a scarcity of research focusing on the impact of constant envelope modulation techniques on the achievable EC in the context of WSNs underpinning SG-IoT.

Against the above backdrop, in this paper, we endeavor to investigate the impact of a constant envelope modulation technique, i.e., continuous phase modulation (CPM), on the EC of sensor nodes in WSNs suitable for SG-IoT. Our novel contributions are summarized as follows.

1. We establish a realistic power consumption model through the analysis of circuit power consumption, transmission power consumption, and reception power consumption on a point-to-point communication link; in particular, we consider three operation modes of the sensors, including sleeping mode, transient mode, and active mode.

2. Based on the above power consumption model and a typical automatic repeat request (ARQ)-based wireless transmission protocol, the EC incurred by successfully sending a single information bit is numerically evaluated under different configurations of CPM parameter values. In particular, we consider different waveform pulses of the CPM, including the rectangular pulse, rising cosine pulse, and GMSK pulse, for comprehensive coverage. We also investigate the impact of the distance between the transmitter and the receiver, the impact of the received SNR, the impact of the modulation order, and the average number of transmissions required for sending a single packet, under various modulation schemes considered.

3. We compare the EC per successfully transmitted bit of the CPM with that of conventional non-constant envelope modulation methods, such as offset quadrature phase-shift keying (OQPSK) used in the Zigbee standard and QAM modulation supported by the current 5G standard. Our simulation results and analysis demonstrate that CPM enjoys a significantly lower EC than OQPSK and 16QAM in the scenario considered, which is valuable for the standard evolution of beyond 5G tailored for the important use case of low-power SG-IoT.

2. The EC Model

To analytically determine the amount of energy consumed when a single bit is transmitted without error, an EC model needs to be established. We make the assumption that each packet transmitted in the forward direction induces an error-free feedback packet in the reverse direction, which acknowledges the successful reception of the data packet or requests for retransmission.

2.1. Packet Structure

In wireless communication systems, the general format of the physical layer packet structure is shown in Figure 1 and consists of three parts: a pilot code for clock synchronization, a packet header specifying the configuration of transmission parameters, and a data payload carrying the transmitted data.
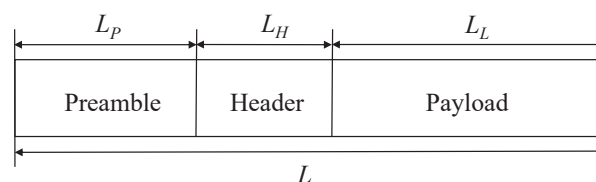

Figure 1. Physical layer packet structure.

We assume that the entire packet uses the same modulation and that the symbol error probability (SEP) is determined by the received SNR γ and the modulation scheme adopted. We also assume that symbol errors are independently and identically distributed (i.i.d.) and no channel coding is used, i.e., no redundant bits are added (redundant bits increase EC). If a symbol is erroneously detected at the receiver, the entire packet will be retransmitted until all the symbols in the packet are correctly detected at the receiver. The packet error

probability (PEP) can be expressed as a function of the SEP, the packet length L, and the number of bits per symbol $m = \log_2 M$, i.e.,

$$\text{PEP} = 1 - (1 - \text{SEP})^{L/m}, \tag{1}$$

where M denotes the size of the modulation constellation.

Hence, by utilizing the packet length L and the probability that a packet is successfully transmitted, i.e., $1 - \text{PEP}$, the average amount of data successfully delivered per transmission duration of a packet is formulated as

$$N_c = L(1 - \text{SEP})^{L/m}. \tag{2}$$

Then, upon assuming that the feedback signal indicating whether a retransmission is needed or not is reliably transmitted on the reverse link, the average number of transmissions required for successfully delivering a packet is given by

$$N_{\text{re}} = \frac{L}{N_c} = \frac{1}{1 - \text{PEP}} = \frac{1}{(1 - \text{SEP})^{L/m}}. \tag{3}$$

2.2. Basics of CPM

CPM is an attractive modulation scheme for WSNs underpinning SG-IoT because its carrier phase is modulated in a continuous manner and it is typically implemented as a constant-envelope waveform, i.e., the transmitted carrier power is constant. The phase continuity requires a relatively small percentage of the power to occur outside of the intended band (e.g., low fractional out-of-band power), leading to high spectral efficiency. Meanwhile, the constant envelope yields excellent power/energy efficiency. However, the primary drawback of CPM is the high implementation complexity required for an optimal receiver.

For systems that employ CPM, the transmitted signal at time instant t can be expressed as [19]

$$s(t, \boldsymbol{I}) = \sqrt{\frac{2E}{T}} \cos(2\pi f_c t + \phi(t, \boldsymbol{I}) + \phi_0), \tag{4}$$

where E is the symbol energy, T is the symbol interval, f_c is the carrier frequency, and ϕ_0 is an arbitrary constant initial phase shift that can be set to zero without loss of generality when coherent transmission is considered. In addition, $\phi(t, \boldsymbol{I})$ is the time-varying information-carrying phase formulated as

$$\phi(t, \boldsymbol{I}) = 2\pi \sum_{k=-\infty}^{K} h_k I_k q(t - kT), KT \leq t \leq (K+1)T, \tag{5}$$

where $\boldsymbol{I} = \{I_k | k \in (-\infty, \cdots, -1, 0, +1, \cdots, K)\}$ is an infinitely long sequence of uncorrelated M-ary data symbols, each having one of the values from the alphabet $\mathcal{A} = \{\pm 1, \pm 3, \cdots, \pm(M-1)\}$ with equal probability $1/M$; $\{h_k\}$ is a sequence of modulation indices defined as $h_k = 2f_{d,k}T$, with $f_{d,k}$ being the peak frequency deviation. When $h_k = h$ for all k, the modulation index remains fixed for all symbols. When the modulation index changes from one symbol to another, the signal is called multi-h CPM, with h_k varying in a cyclic manner. $q(t)$ is some normalized waveform shape that represents the baseband phase response (i.e., phase pulse) and is obtained from the frequency pulse $g(t)$ by

$$q(t) = \int_{-\infty}^{t} g(\tau) d\tau. \tag{6}$$

If the duration of $g(t)$ is equal to the symbol interval T, namely, $g(t) = 0$ for $t > T$, the modulated signal is called full-response CPM. If the duration of $g(t)$ is larger than

the symbol interval T, namely, $g(t) \neq 0$ for $t > T$, the modulated signal is called partial-response CPM.

Suppose the length of the frequency pulse $g(t)$ in terms of the number of symbol intervals is N. Thus, $N = 1$ yields full-response CPM. If $g(t)$ is selected as a rectangular pulse, namely,

$$g(t) = \begin{cases} \frac{1}{2NT}, & 0 \leq t \leq NT, \\ 0, & \text{otherwise,} \end{cases} \tag{7}$$

then for a full-response CPM, we have

$$q(t) = \begin{cases} 0, & t \leq 0, \\ \frac{t}{2T}, & 0 \leq t \leq T, \\ \frac{1}{2}, & t \geq T. \end{cases} \tag{8}$$

It is evident that the performance of CPM is influenced by certain parameters, including but not limited to M, h_k, N, and the frequency pulse $g(t)$. Note that by choosing different pulse shapes $g(t)$ and varying M, h_k, and N, an infinite variety of CPM signals may be generated, each with its unique characteristics and performance.

For a CPM signal, the error rate performance can be derived based on the maximum-likelihood sequence detection (MLSD) receiver, which is conventionally computed using the Viterbi Algorithm (VA). Specifically, for a given CPM scheme, we have

$$\mathsf{SEP} = K_{\min} Q\left(\sqrt{d_{\min}^2 \gamma}\right). \tag{9}$$

According to Anderson's seminal work on digital phase modulation [20], $K_{\min}$ denotes the total number of feasible paths that satisfy the constraint of the minimum Euclidean distance $d_{\min}$ within the observation interval on the CPM phase grid. The value of $K_{\min}$ increases with the modulation order M. Both $K_{\min}$ and $d_{\min}$ depend on critical parameters including M, h_k, N, and the pulse shaping function $g(t)$.

2.3. Circuit Power Consumption

In wireless communication systems, a significant portion of energy is dedicated to signal transmission and reception circuits, which are mainly composed of the baseband (BB) digital signal processing unit and the radio frequency (RF) signal processing unit, as shown in Figure 2. To elaborate a little further, the BB signal processing unit mainly includes source coding/decoding, pulse shaping, channel coding/decoding, digital modulation/demodulation, channel estimation, synchronization, and so on. For a wireless sensor, since the data rate requirement is usually low, the BB symbol rate is also low. Meanwhile, typically, no computation-intensive signal processing techniques, such as multi-user detection and iterative decoding, are used in an energy-constrained wireless sensor; hence, the BB power consumption is significantly smaller than the RF circuit power consumption.

A typical model of an RF signal processing unit, also known as an RF chain, is shown in Figure 3 [14,16,21–23]. Specifically, on the transmitter side, the BB signal is first converted to an analog signal by the digital-to-analog converter (DAC). Then, the analog signal is filtered by the low-pass filter and upconverted by the mixer, whose output is then filtered again, amplified by the power amplifier (PA), passed through the duplexer, and finally transmitted to the wireless channel. On the receiver side, the RF signal is sequentially filtered, amplified by the low-noise amplifier (LNA), cleaned by the anti-aliasing filter, downconverted by the mixer, filtered again before passing through the intermediate frequency amplifier (IFA) that has an adjustable gain, and finally converted back to a digital signal by the analog-to-digital converter (ADC). Note that the mixers operate with the aid of the local oscillator (LO) and, among all the RF components, the PA and LNA usually have much higher power consumption than the others.
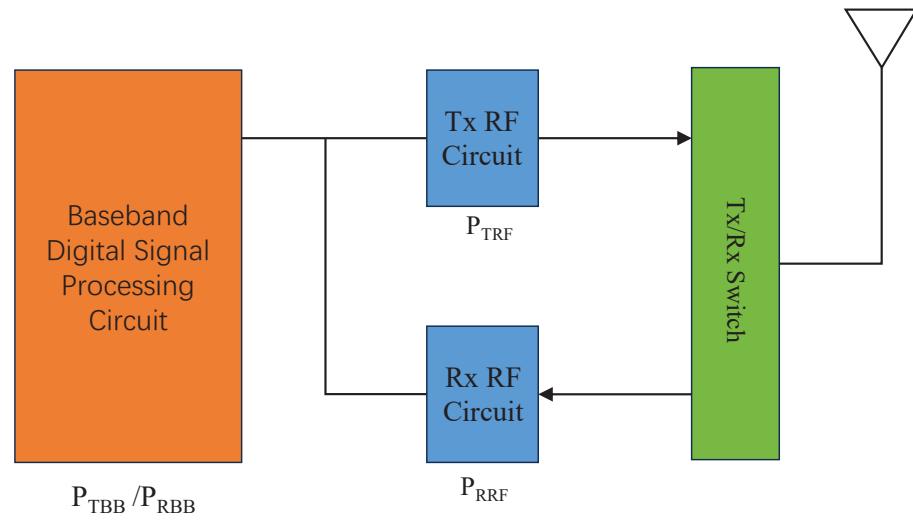
Figure 2. The communication modules and the corresponding power consumption model of a point-to-point wireless communication system.
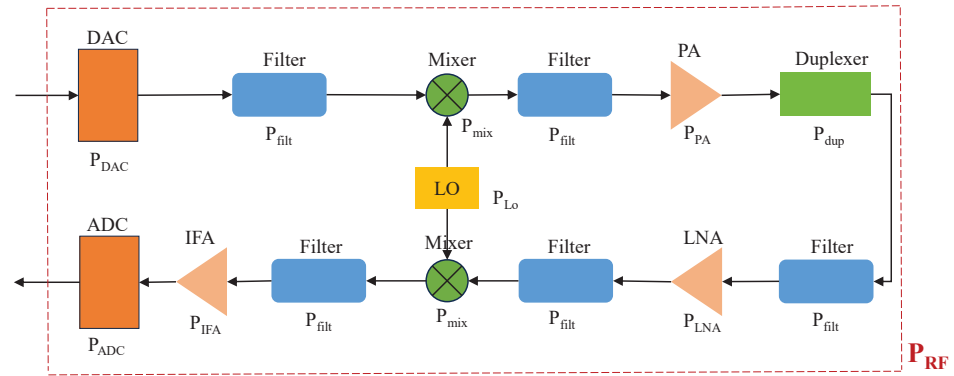

Figure 3. A typical power consumption model of the RF signal processing unit of a point-to-point wireless communication system.

Accordingly, the total power consumption during transmission can be expressed as

$$P_{Tx}(d) = P_{TBB} + \underbrace{P_{TRF} + P_{PA}(d)}_{P_{TRF}} = P_{T0} + \frac{\xi}{\eta} P_T(d), \tag{10}$$

where P_{TBB} and P_{TRF} represent the power consumption of the transmitter's BB processing unit and RF processing unit excluding the PA, respectively, and both of them can be regarded as constant values that are collectively denoted by P_{T0}; $P_{PA}(d)$ and $P_T(d)$ are defined as the power consumption of the PA and the transmit power, respectively, both of which are functions of the transmission distance d upon assuming adaptive power control and are related via $P_{PA}(d) = \frac{\xi}{\eta} P_T(d)$; and η and ξ represent the drain efficiency and the peak-to-average power ratio (PAPR) of the PA, respectively [18].

Similarly, the total power consumption of the receiver is expressed as

$$P_{Rx} = P_{RBB} + \underbrace{P_{RRF} + P_{LNA}}_{P_{RRF}} = P_{R0}, \tag{11}$$

where P_{RBB} and P_{RRF} represent the power consumption of the receiver's BB processing unit and RF processing unit excluding LNA, respectively, and both of them can be regarded as constant values; P_{LNA} represents the power consumption of the LNA, which is also constant upon assuming that the LNA is appropriately designed and biased, so that

necessary sensitivity is provided for reliably receiving, demodulating, and decoding a minimum power signal. Hence, P_{RBB}, P_{RRF}, and P_{LNA} are collectively denoted by the constant P_{R0}.

2.4. Transmission Power Consumption

Due to the path-loss, scattering, reflection, and other phenomena in the wireless channel, a certain amount of energy is inevitably lost during the transmission of electromagnetic waves that carry data symbols, thus resulting in transmission energy dissipation. The path-loss depends on several factors, such as the distance between the transmitter and receiver, the frequency of the signal, the type of antennas used, and the environment through which the signal propagates.

When the signal with a transmit power $P_T(d)$ is propagated through the wireless channel, the received power $P_R(d)$ at the receiver can be formulated as

$$P_R(d) = G_T G_R P_T(d) \left(\frac{\lambda}{4\pi d}\right)^\alpha = \frac{P_T(d)}{A_0 d^\alpha}, \tag{12}$$

according to Friis' transmission equation. This expression characterizes the dependency between the received power with respect to several parameters. Specifically, the constant A_0 depends on the transmit antenna gain G_T, the receive antenna gain G_R, and the carrier wavelength λ. Additionally, the path-loss exponent is α. It is noted that the received power is inversely proportional to the distance d raised to the power of α, and the received SNR γ is proportional to $1/A_0$ divided by d^α. These relationships collectively describe how the aforementioned parameters influence the received power and the received SNR [18]:

$$\gamma = \frac{P_R(d)}{N_0 W N_f M_l}, \tag{13}$$

where W represents the transmission bandwidth, N_0 denotes the power spectral density of the baseband-equivalent additive white Gaussian noise (AWGN), and they are primary determinants of γ. Furthermore, the noise figure of the RF front-end of the receiver, denoted as N_f, and any additional noise or interference, represented by the link margin term M_l, can also impact the received SNR γ.

Accordingly, by substituting Equation (12) into Equation (13), the relationship between the transmit power $P_T(d)$, the communication distance d, the received SNR γ, and other parameters can be quantitatively expressed as

$$P_T(d) = A_0 d^\alpha N_0 W N_f M_l \gamma = A d^\alpha \gamma, \tag{14}$$

where we have $A = A_0 N_0 W N_f M_l$.

2.5. EC per Successfully Transmitted Bit

As mentioned in Section 2, we assume that each packet transmitted in the forward direction is matched by an error-free feedback packet in the reverse direction in order to guarantee reliable transmission. Both directions of transmissions consume energy. The above transmission process, usually incorporating retransmissions, continues until the entire packet of the forward direction is correctly decoded at the receiver. Additionally, we assume that the sensor node transceiver circuitry works in a multi-mode manner: (1) when there are data to transmit or receive, all circuits of the sensor work in the active mode; (2) when neither transmission nor reception are needed, the circuits of the sensor enter sleep mode by default, which uses the minimum possible power (small enough to be negligible) to ensure that the circuits can be activated when necessary; (3) when the sensor is in the period of switching from sleep mode to active mode, it is in a transient mode that also consumes non-negligible energy. Note that the transient duration from active mode to sleep mode is sufficiently short to be neglected but the start-up process from sleep mode to active mode can be slow.

Therefore, for a single round-trip transmission (forward direction transmission and reverse direction feedback) on a point-to-point communication link, the total EC of the system can be divided into two parts: the EC of the forward direction transmission and the EC of the reverse direction feedback. For the forward direction transmission, the EC is composed of the start-up energy consumption $2E_{ST}$ in transient mode (both the transmitting node and the receiving node may be in sleep mode initially), the transmitter energy consumption $E_{Tx}(d)$ in active mode, and the receiver energy consumption E_{Rx} in active mode. Therefore, the EC of the forward direction transmission is expressed as

$$E_{FW} = 2E_{ST} + E_{Tx}(d) + E_{Rx} = 2E_{ST} + P_{Tx}(d)T_{DTA} + P_{Rx}T_{DRA}, \tag{15}$$

where T_{DTA} is the transmission duration for sending a data packet in the forward direction and T_{DRA} is the corresponding duration of signal processing at the receiver of the forward direction.

Additionally, the EC of the reverse direction transmission is expressed as

$$E_{RV} = \underline{P}_{Tx}(d)T_{FTA} + P_{Rx}T_{FRA}, \tag{16}$$

where $\underline{P}_{Tx}(d)$ is the total power consumption for transmission of a feedback packet in the reverse direction by the receiving node of the forward direction and T_{FTA} is the corresponding time duration. Note that $\underline{P}_{Tx}(d)$ may be different from $P_{Tx}(d)$ of the forward direction because a feedback packet may have a different transmission rate and reliability requirements compared with a data packet. T_{FRA} is the duration of processing the feedback packet at its receiver (i.e., the transmitting node of the forward direction) in active mode.

Based on the above analysis, we obtain the EC per successfully transmitted bit as

$$
\begin{aligned}
E_b &= \frac{N_{re}(E_{FW} + E_{RV})}{L} \\
&= \frac{E_{FW} + E_{RV}}{N_c} \\
&= \frac{2E_{ST} + P_{Tx}(d)T_{DTA} + P_{Rx}T_{DRA} + \underline{P}_{Tx}(d)T_{FTA} + P_{Rx}T_{FRA}}{L(1 - \mathsf{SEP})^{L/m}} \\
&= \frac{2E_{ST} + (P_{T0} + \frac{\xi}{\eta}P_T(d))T_{DTA} + P_{Rx}T_{DRA} + (P_{T0} + \frac{\xi}{\eta}\underline{P}_T(d))T_{FTA} + P_{Rx}T_{FRA}}{L(1 - K_{min}Q(\sqrt{d_{min}^2\gamma}))^{L/m}},
\end{aligned} \tag{17}
$$

where $\underline{P}_T(d)$ is the transmit power for the feedback packet transmission and N_{re} is the average number of retransmissions.

3. CPM Parameter Selection

As mentioned in Section 2.2, the main parameters that affect the performance of CPM are M, h_k, N, and the frequency pulse shaping function $g(t)$, whilst the minimum squared Euclidean distance d_{min}^2 also depends on these parameters. Therefore, it is necessary to determine how these parameters influence the EC per successfully transmitted bit.

In principle, it is possible to implement an infinite number of different CPM signals using various combinations of design parameters. However, for practical implementation, we must consider the trade-off between the achievable performance and the cost incurred. It is well known that partial-response CPM signals usually have better spectral efficiency than full-response CPM signals. However, the computational complexity of the optimal MLSD receiver exponentially increases with N, which is the length of $g(t)$ in terms of the number of symbol intervals. In this study, we focus on the partial-response CPM with a moderate value of $N = 3$. The modulation order M also significantly influences the computational complexity and the requirements for demodulation devices [24], which can lead to high EC. Therefore, small values, such as $M = 2, 4, 8, 16$, etc., are generally chosen. We assume the modulation index $h_k = h$, which is also an important parameter

and has a complex functional relationship with the minimum squared Euclidean distance $d_{\min}^2$ [24,25]. Smaller values of h result in narrower bandwidth, more concentrated signal energy, and narrower transition bands. However, they also make the phase variations less obvious and can increase the complexity of demodulation decisions. For single index modulation, $h = 0.5$ or 0.75 is commonly used. Finally, the pulse shaping function $g(t)$ usually utilizes rectangular pulse (REC), rising cosine pulse (RC), and Gauss minimum-phase shift-keying pulse (GMSK) [26].

Given the imperative to minimize EC for sensors, the present study focuses on CPM signals that can be implemented with simple devices and require low computational complexity. Accordingly, CPM signals with three different $g(t)$ functions are selected for investigation, assuming $M = 2, 4, 8, 16$, $h = 0.75$, and $N = 3$. The values of $d_{\min}^2$ under these parameter configurations are calculated with the methods given in [24,25] and listed in Table 1.

Table 1. The value of $d_{\min}^2$ when we set $M = 2, 4, 8, 16$, $h = 0.75$, and $N = 3$. For GMSK, the time-bandwidth product BT is set to 0.3, where B is the -3 dB bandwidth of the Gaussian pulse.

Waveform	$M = 2$	$M = 4$	$M = 8$	$M = 16$
REC	2.31648	1.41550	2.12325	2.831
RC	2.96059	5.30037	6.12447	8.16596
GMSK	2.89955	4.69275	5.95011	7.93348

4. Evaluation the EC of CPM

4.1. Identification of Major Performance Influencing Factors

From Equation (17), it can be observed that the EC per successfully transmitted bit, E_b, is predominantly determined by four parameters: the forward-link transmit power $P_T(d)$, the reverse-link transmit power $\underline{P}_T(d)$, the specific CPM scheme adopted, and the received SNR γ. From another perspective, we can also say that E_b is mainly determined by $P_T(d)$, $\underline{P}_T(d)$, the achievable SEP, and the modulation efficiency m. Upon inspection of Equations (13) and (9), it becomes clear that the SEP on the forward link can be expressed as

$$\text{SEP} = K_{\min} Q\left(\sqrt{d_{\min}^2 \frac{P_T(d)}{A_0 d^\alpha N_0 W N_f M_l}} \right). \tag{18}$$

Although a high transmit power is desirable for achieving a low SEP and thus reducing the number of retransmissions N_{re}, it may also result in excessively large transmission power for the sensor and increase the EC of each single-direction transmission. Hence, an optimal transmit power (or in turn the received SNR γ) exists and is yet to be found for minimizing the EC per successfully transmitted bit. Similarly, the relationship between the EC per successfully transmitted bit and other major parameters mentioned above needs to be studied.

4.2. Simulation Results and Discussions

In the following numerical simulations, we consider the radio links of a WSN designed for smart grid and operating in the industrial–science–medical (ISM)-oriented 2.4 GHz frequency band. Table 2 provides a summary of the pertinent simulation parameters, including circuit-related parameter settings as well. Due to the constant envelope characteristic of the CPM signal, a nonlinear PA with a high η value is employed, in contrast to the general radio architecture.

Table 2. A summary of the pertinent simulation parameters.

Parameters	Values
Symbol rate for transmitted signals	20 ksps
L_P, L_H, and L_L	4, 3, and 30 bytes
Power spectral density of AWGN at the receiver (N_0)	−174 dBm/Hz
Noise figure of the RF front-end of the receiver (N_f)	10 dB
Equivalent antenna gain (A_0)	30 dB
Bandwidth (W)	20 kHz
Additional noise (M_l)	10 dB
P_{T0}	15.9 mW
P_{R0}	58.2 mW
M	2, 4, 8, 16
h	0.75
N	3
Path-loss exponent (α)	3.5
Drain efficiency (η)	0.7 for CPM; 0.35 for OQPSK and 16QAM
Peak-to-average power ratio (ξ)	0 dB for CPM; 3.5 dB for OQPSK; 6.7 dB for 16QAM

First, let us compare the EC performance of different CPM schemes and of other representative modulation schemes, such as OQPSK and 16QAM, by observing how E_b varies with the received SNR γ. As shown in Figure 4, for all modulation schemes, the achievable E_b values firstly descend and then increase with the received SNR. This is because in the low-SNR region, the number of retransmissions plays an important role, while the number of retransmissions is reduced to its minimum under a sufficiently high SNR, and then an even higher SNR means unnecessary energy wastage. In addition, for most SNRs, the achievable E_b values of REC ($d_{\min}^2 = 2.831$, $h = 0.75$ and $N = 3$), RC ($d_{\min}^2 = 8.16596$, $h = 0.75$ and $N = 3$), and GMSK ($d_{\min}^2 = 7.93348$, $h = 0.75$ and $N = 3$) are lower than those of OQPSK and 16QAM, which verifies the advantages of CPM in terms of energy saving. The reason why a higher order CPM scheme has a lower E_b can be explained by referring to Equation (17) as follows: (1) a larger M causes a smaller number of symbols per packet (i.e., the smaller exponent L/m) and a smaller SEP (i.e., the larger base number $1 - \text{SEP}$), thus the denominator $L(1 - \text{SEP})^{L/m}$ increases with M; (2) the variable T_{DTA} in the numerator becomes smaller when M becomes larger, while all the other terms can be regarded as constants. Furthermore, we can see that the lowest values of E_b achieved by the four modulation schemes having $M = 16$ (i.e., REC, RC, GMSK, and 16QAM) are almost the same, while OQPSK having $M = 4$ achieves the largest E_b in the high-SNR region and the second-largest E_b in the low-SNR region. It is also observed that when the SNR is above a specific threshold, the three different CPM waveforms exhibit the same EC performance.

Figure 5 characterizes the relationship between E_b and the communication distance d for OQPSK, 16QAM, and the CPM signals with different pulse shaping functions. We can see that E_b increases with d for all the modulation schemes considered. This is because large distance reduces the received SNR value under a given transmit power, thus degrading the SEP performance and increasing the number of retransmissions. We also see that all the three CPM waveforms considered have the same EC performance curves, which are consistently and significantly better than those of OQPSK and 16QAM when d is sufficiently large. Here, we assume $\gamma = 8$ dB for the three CPM waveforms and $\gamma = 15$ dB for OQPSK and 16QAM. The two SNR values are selected according to the results shown in Figure 4, where the three CPM waveforms achieve their optimal E_b at about $\gamma = 8$ dB, while OQPSK and 16QAM achieve their near-optimal E_b at about $\gamma = 15$ dB.
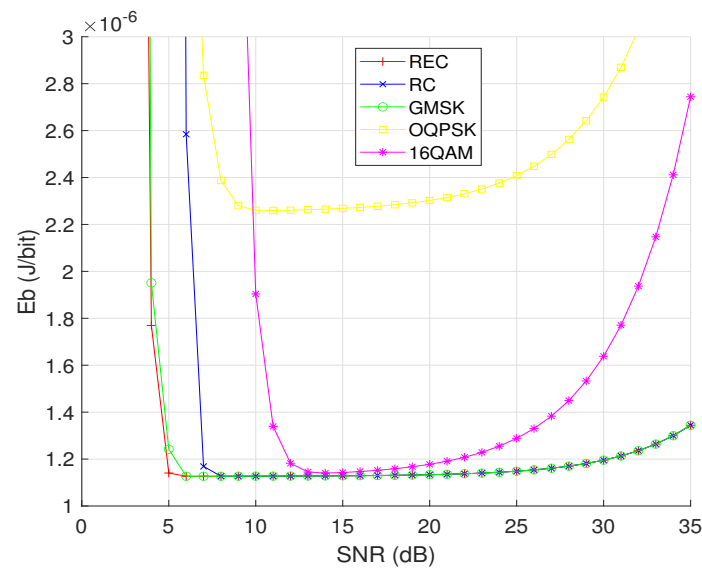
Figure 4. The relationship between the EC per successfully transmitted bit (E_b) and the received SNR (γ) for OQPSK, 16QAM, and the CPM signals with different pulse shaping functions (REC, RC, and GMSK), while assuming $M = 16$ and $N = 3$ for the three CPM waveforms, as well as $d = 10$ m and the AWGN channel for all the modulation schemes considered.
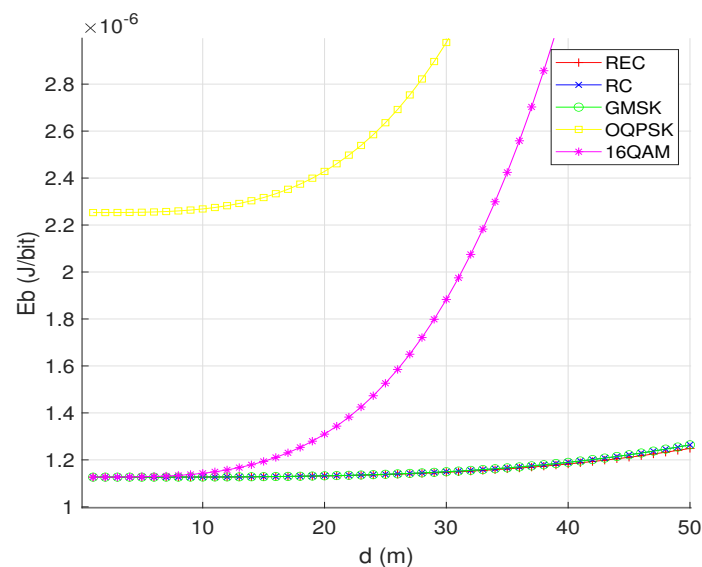

Figure 5. The relationship between the EC per successfully transmitted bit (E_b) and the communication distance (d) for OQPSK, 16QAM, and the CPM signals with different pulse shaping functions (REC, RC, and GMSK) o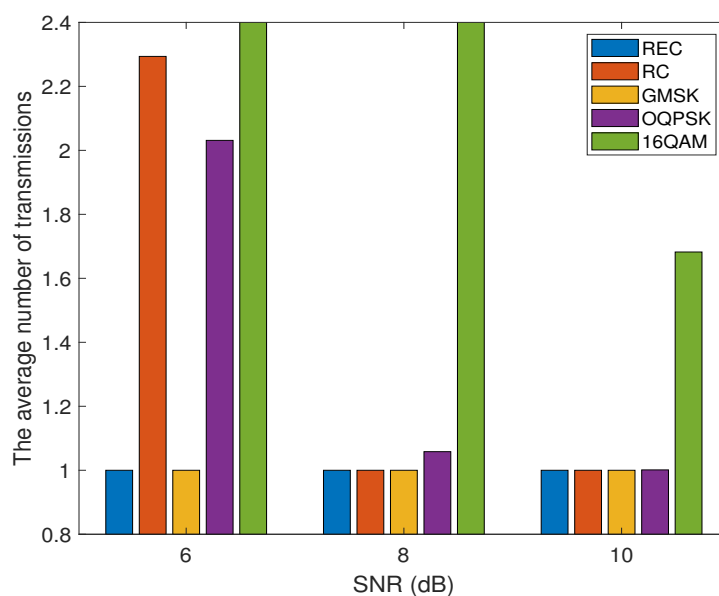ver the AWGN channel, while assuming $M = 16$, $N = 3$ and $\gamma = 8$ dB for the three CPM waveforms, as well as $\gamma = 15$ dB for OQPSK and 16QAM signals.

Figure 6 shows how the E_b values of the three CPM waveforms vary with the modulation efficiency m, while assuming $\gamma = 8$ dB and $d = 10$ m. It is observed that for each given CPM waveform, the E_b value becomes smaller as m increases. Although the RC-based CPM signaling exhibits the highest E_b when $m = 1, 2, 3$, all the three CPM waveforms achieve almost the same E_b when $m = 4$ (i.e., $M = 16$). This is because the three CPM waveforms achieve almost the same SEP performance when $m = 4$, $\gamma = 8$ dB, and $d = 10$ m. These observations are consistent with the results shown in Figure 4.

Figure 7 demonstrates the relationship between the average number of transmissions N_{re} required for successfully sending a single packet and the received SNR γ over the AWGN channel employing different modulation schemes, including OQPSK, 16QAM, and

the three CPM waveforms. Obviously, 16QAM incurs the largest N_{re}, while the REC- and GMSK-based CPM schemes require the smallest N_{re}, under all the three SNR values of 6 dB, 8 dB, and 10 dB. In addition, the OQPSK scheme requires a smaller and a larger N_{re} than the RC-based CPM scheme under $\gamma = 6$ dB and $\gamma = 8$ dB, respectively. However, when the received SNR is sufficiently high, e.g., $\gamma = 10$ dB, all the modulation schemes, except 16QAM, require only a single transmission on average for successfully sending a packet.

Figure 6. The relationship between the EC per successfully transmitted bit (E_b) and the modulation efficiency *m* for the CPM signals with different pulse shaping functions (REC, RC, and GMSK) over the AWGN channel, while assuming $N = 3$, $\gamma = 8$ dB and $d = 10$ m.

Figure 7. The relationship between the average number of transmissions required for successfully sending a single packet and the received SNR (γ), while considering OQPSK, 16QAM, and the CPM signals with different pulse shaping functions (REC, RC, and GMSK) over the AWGN channel. Assume that $M = 16$ and $N = 3$ for the three CPM waveforms, and $d = 10$ m for all the modulation schemes compared.

5. Conclusions

In this paper, the EC characteristics of various CPM schemes are compared with those of OQPSK and 16QAM in the context of WSN-based SG-IoT of beyond 5G. We first propose an EC model for the sensor nodes of WSNs by considering the circuits and a typical communication protocol that relies on ARQ-based retransmissions. Our analytical and simulation results demonstrate that all the CPM schemes based on the pulse shaping functions of REC, RC, and GMSK significantly outperform OQPSK used in the Zigbee standard and 16QAM used in the current 5G standard, in terms of the EC per successfully transmitted bit, E_b. We also show that for all the modulation schemes considered, the individual optimum values of E_b are achieved with the received SNR that is neither too small nor too large. In addition, we show that E_b increases with the communication distance d for all the modulation schemes considered, and decreases with the modulation order M for the three CPM schemes. Overall, it is observed that the REC- and GMSK-based CPM schemes achieve the best EC performance of all the modulation schemes considered.

Data Availability Statement: No new data were created or analyzed in this study. Data sharing is not applicable to this article.

Conflicts of Interest: The authors declare no conflicts of interest. The funders had no role in the design of the study; in the collection, analyses, or interpretation of data; in the writing of the manuscript; or in the decision to publish the results.

References

1. Fei, Z.; Li, B.; Yang, S.; Xing, C.; Chen, H.; Hanzo, L. A survey of multi-objective optimization in wireless sensor networks: Metrics, algorithms, and open problems. *IEEE Commun. Surv. Tutor.* **2017**, *19*, 550–586. [CrossRef]
2. Cao, H.; Du, J.; Zhao, H.; Luo, D.X.; Kumar, N.; Yang, L.; Yu, F.R. Toward tailored resource allocation of slices in 6G networks with softwarization and virtualization. *IEEE Internet Things J.* **2022**, *9*, 6623–6637. [CrossRef]
3. Cheung, K.T.K.; Yang, S.; Hanzo, L. Achieving maximum energy-efficiency in multi-relay OFDMA cellular networks: A fractional programming approach. *IEEE Trans. Commun.* **2013**, *61*, 2746–2757. [CrossRef]
4. Cheung, K.T.K.; Yang, S.; Hanzo, L. Maximizing energy-efficiency in multi-relay OFDMA cellular networks. In Proceedings of the IEEE Global Communications Conference (GLOBECOM'13), Atlanta, GA, USA, 9–13 December 2013; pp. 2767–2772.
5. Cheung, K.T.K.; Yang, S.; Hanzo, L. Spectral and energy spectral efficiency optimization of joint transmit and receive beamforming based multi-relay MIMO-OFDMA cellular networks. *IEEE Trans. Wirel. Commun.* **2014**, *13*, 6147–6165. [CrossRef]
6. Jing, W.; Lu, Z.; Wen, X.; Hu, Z.; Yang, S. Flexible resource allocation for joint optimization of energy and spectral efficiency in OFDMA multi- cell networks. *IEEE Commun. Lett.* **2015**, *19*, 451–454. [CrossRef]
7. Cheung, K.T.K.; Yang, S.; Hanzo, L. Distributed energy spectral efficiency optimization for partial/full interference alignment in multi- user multi-relay multi-cell MIMO systems. *IEEE Trans. Signal Process.* **2016**, *64*, 882–896. [CrossRef]
8. Tan, F.; Lv, T.; Yang, S. Power allocation optimization for energy- efficient massive MIMO aided multi-pair decode-and-forward relay systems. *IEEE Trans. Commun.* **2017**, *65*, 2368–2381. [CrossRef]
9. Miao, X.; Yang, S.; Wang, C.; Wang, S.; Hanzo, L. On the energy efficiency of interference alignment in the *K*-user interference channel. *IEEE Access* **2019**, *7*, 97253–97263. [CrossRef]
10. Abrão, T.; Sampaio, L.D.H.; Yang, S.; Cheung, K.T.K.; Jeszensky, P.J.E.; Hanzo, L. Energy efficient OFDMA networks maintaining statistical QoS guarantees for delay-sensitive traffic. *IEEE Access* **2016**, *4*, 774–791. [CrossRef]
11. Zhao, L.; Yang, S.; Chi, X.; Chen, W.; Ma, S. Achieving energy-efficient uplink URLLC with MIMO-aided grant-free access. *IEEE Trans. Wirel. Commun.* **2022**, *21*, 1407–1420. [CrossRef]
12. Lin, Z.; Lin, M.; Champagne, B.; Zhu, W.-P.; Al-Dhahir, N. Secrecy-energy efficient hybrid beamforming for satellite-terrestrial integrated networks. *IEEE Trans. Commun.* **2021**, *69*, 6345–6360. [CrossRef]

13. Lin, Z.; An, K.; Niu, H.; Hu, Y.; Chatzinotas, S.; Zheng, G.; Wang, J. SLNR-based secure energy efficient beamforming in multibeam satellite systems. *IEEE Trans. Aerosp. Electron. Syst.* **2023**, *59*, 2085–2088. [CrossRef]
14. Cui, S.; Goldsmith, A.J.; Bahai, A. Energy-constrained modulation optimization. *IEEE Trans. Wirel. Commun.* **2005**, *4*, 2349–2360.
15. Rosas, F.; Oberli, C. Modulation optimization for achieving energy efficient communications over fading channels. In Proceedings of the IEEE 75th Vehicular Technology Conference (VTC Spring'12), Yokohama, Japan, 6–9 May 2012; pp. 1–5.
16. Wang, T.; Heinzelman, W.B.; Seyedi, A. Minimization of transceiver energy consumption in wireless sensor networks with AWGN channels. In Proceedings of the 46th Annual Allerton Conference on Communication, Control, and Computing (Allerton'08), Monticello, IL, USA, 23–26 September 2008; pp. 62–66.
17. Abo-Zahhad, M.; Farrag, M.; Ali, A. Modeling and minimization of energy consumption in wireless sensor networks. In Proceedings of the IEEE International Conference on Electronics, Circuits, and Systems (ICECS'15), Cairo, Egypt, 6–9 December 2015; pp. 697–700.
18. Rosas, F.; Oberli, C. Modulation and SNR optimization for achieving energy-efficient communications over short-range fading channels. *IEEE Trans. Wirel. Commun.* **2012**, *11*, 4286–4295. [CrossRef]
19. Aulin, T.; Sundberg, C.E. Continuous phase modulation—Part I: Full response signaling. *IEEE Trans. Commun.* **1981**, *29*, 196–209. [CrossRef]
20. Anderson, J.B.; Aulin, T.; Sundberg, C.E. *Digital Phase Modulation*; Plenum Press: New York, NY, USA, 1986.
21. Amin, O.; Bavarian, S.; Lampe, L. Cooperative techniques for energy-efficient wireless communications. In *Green Radio Communication Networks*; Hossain, E., Bhargava, V.K., Fettweis, G.P., Eds.; Cambridge University Press: Cambridge, UK, 2012; Chapter 6, pp. 125–149.
22. Wang, Q.; Hempstead, M.; Yang, W. A realistic power consumption model for wireless sensor network devices. In Proceedings of the 3rd Annual IEEE Communications Society Conference on Sensor, Mesh and Ad Hoc Communications and Networks (SECON'06), Reston, VA, USA, 25–28 September 2006; pp. 286–295.
23. Zhang, S.; Xu, S.; Li, G.Y.; Ayanoglu, E. First 20 years of green radios. *IEEE Trans. Green Commun. Netw.* **2020**, *4*, 1–15. [CrossRef]
24. Aulin, T.; Rydbeck, N.; Sundberg, C.E. Continuous phase modulation—Part II: Partial response signaling. *IEEE Trans. Commun.* **1981**, *29*, 210–225. [CrossRef]
25. Kassan, K.; Farès, H.; Glattli, D.C.; Louët, Y. Performance vs. spectral properties for single-sideband continuous phase modulation. *IEEE Trans. Commun.* **2021**, *69*, 4402–4416. [CrossRef]
26. Foruhandeh, M.; Uysal, M.; Altunbas, I.; Guven, T.; Gercek, A. Optimal choice of transmission parameters for LDPC-coded CPM. In Proceedings of the IEEE Military Communications Conference (MILCOM'14), Baltimore, MD, USA, 6–8 October 2014; pp. 368–371.